Supporting Figures

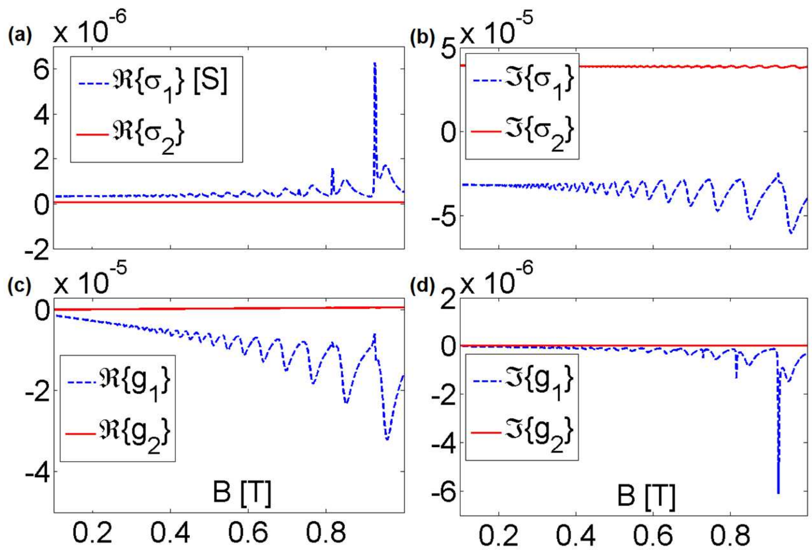

Supporting Figure 1. Typical conductivities behavior as a function of $\mathbf{B}_{dc}$ at the fixed frequency 46.2THz and with T=3K, $\Gamma = 0.43meV$, $\mu_{c_1} = 0.1\text{eV}$ and $\mu_{c_1} = 0.16\text{eV}$.

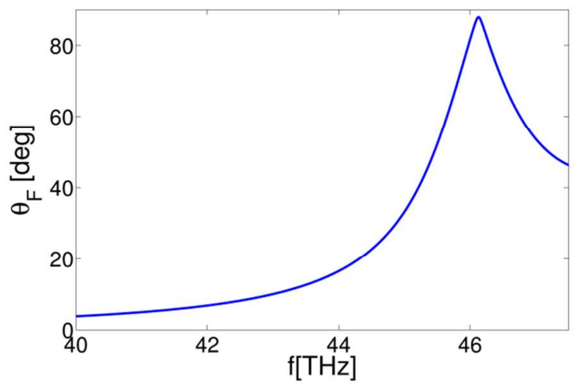

Supporting Figure 2. The total field in the interruption location is rotated by 87 degrees at resonance with respect to the incident field polarization.

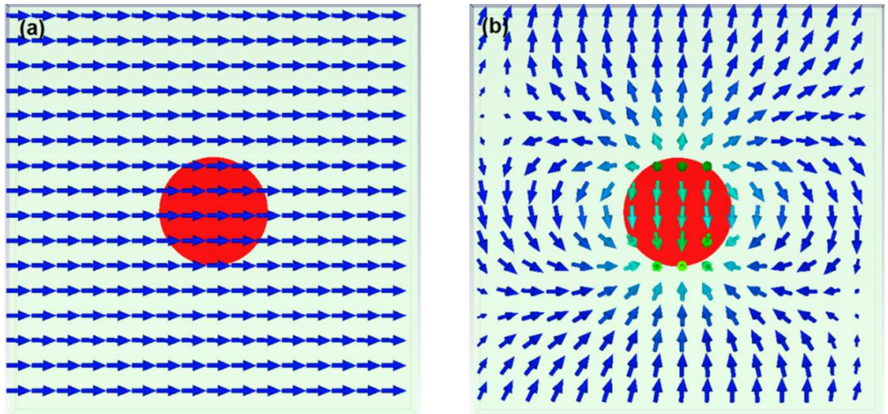

Supporting Figure 3. The electric field as calculated by CST. Resonance frequency f=43.361THz – it is red shifted compare to the analytic result due to retardation effects caused by the interruption's finite size (**a**) the E-field far from the graphene surface - it is x-polarized (**b**) The E field very close to the graphene surface – y-polarized dipole field. Note also the color map - the fields close to the interruption are two orders of magnitude stronger than the incident field.

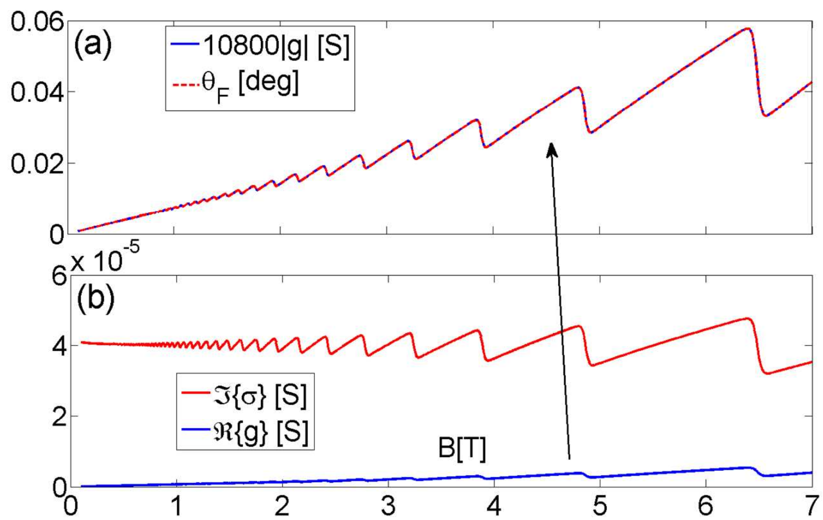

Supporting Figure 4. The rotation angle due to suspended, homogeneous graphene layer with $\mu_{c_1} = 0.1\mathrm{eV}$, T=3K, $\Gamma = 0.43\mathrm{meV}$, and f=46.2THz, as a function of the bias magnetic field - up to B=7T. (a) The rotation angle calculated by Eq. 15 in the Supporting Information (dashed line) and approximated by Eq. 16 there (solid line). It is clearly seen that the approximate result in Eq. 16 holds well and the rotation follows the conductivity. (b) The imaginary part of the diagonal (red) and the real part of the off-diagonal (blue) terms of the conductivity. These are the dominant terms in the conductivity tensor.

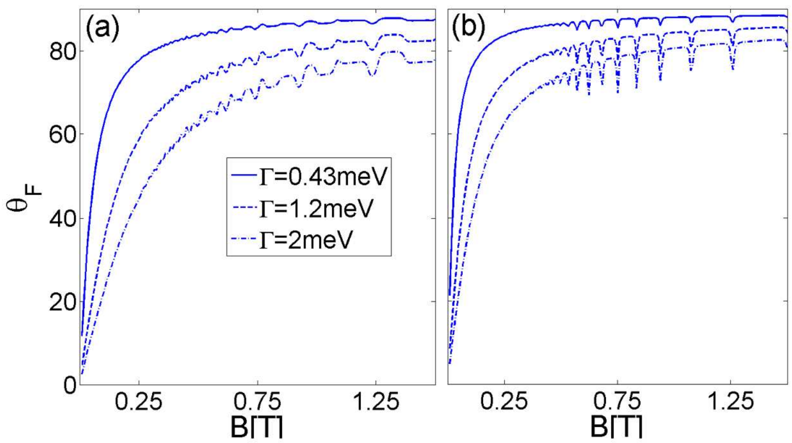

Supporting Figure 5. The *maximal* rotation angle in the near field as function of the magnetic bias field, and for interruption diameter of 8nm, calculated using Eq. 1 in the main text. Note that this figure does not correspond to a specific single frequency; at each value of B the frequency at which the rotation angle is maximal was found and the corresponding angle was plotted against B, i.e. $\theta_F(B) = \max_f[\theta(B,f)]$. The scattering rate is a parameter. (a) Results for $\mu_{c_1} = 0.1\text{eV}, \mu_{c_2} = 0.12\text{eV}$ (b) Results for $\mu_{c_1} = 0.1\text{eV}, \mu_{c_2} = 0.16\text{eV}$.

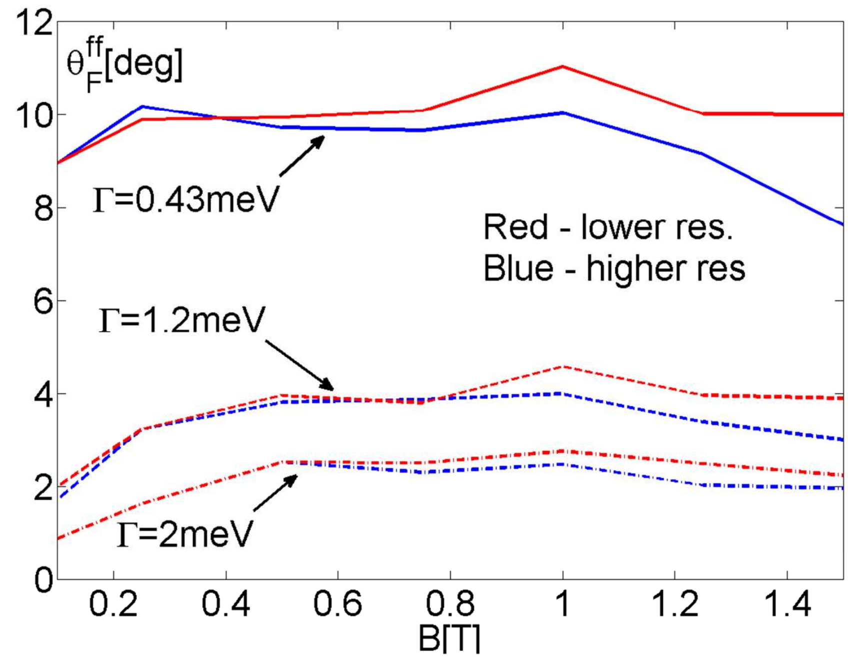

Supporting Figure 6. The *maximal* rotation angle in the far field as function of the bias magnetic field as obtained by CST simulations, for $\mu_{c_1} = 0.1\mathrm{eV}, \mu_{c_2} = 0.16\mathrm{eV}$, T=3K, $\Gamma = 0.43, 1.2, 2\,\mathrm{meV}$, D=8nm, a=b=12nm. Two colors for the two resonances - blue - lower, red - higher. Note that as in **Supporting Figure 5**, this figure was not calculated at specific frequency but for each magnetic bias, B point we found the frequency at which the rotation angle is maximal and took its value, i.e. $\theta_F(B) = \max_f[\theta(B,f)]$.

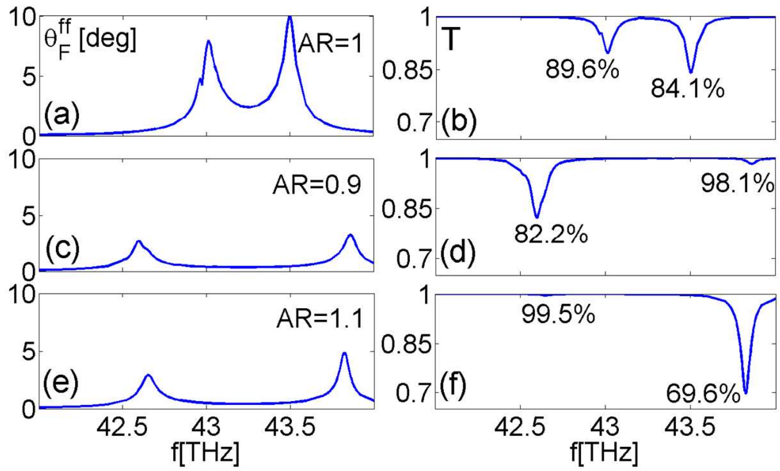

Supporting Figure 7. Elliptical interruptions arranged in a square lattice with $\mu_{c_1} = 0.1\text{eV}, \mu_{c_2} = 0.16\text{eV}$, T=3K, $\Gamma = 0.43\text{meV}$, a=b=12nm, B=1.5T. (**a**,**b**) Faraday rotation angle in the far-field and transmission coefficient vs. frequency for circular interruptions of D=8nm. (**c**,**d**) The same as previous ones but with elliptical interruption with $R_y / R_x = 0.9$ and $R_x R_y = R^2$ - same fill factor as for the circular case. (**e**,**f**) The same as previous one but with $R_y / R_x = 1.1$ and $R_x R_y = R^2$- same fill factor as for the circular case.

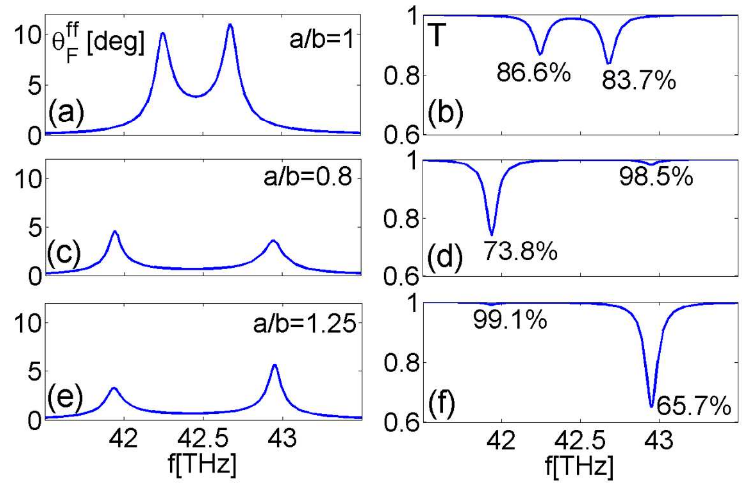

Supporting Figure 8. Circular interruptions arranged in a rectangular lattice with $\mu_{c_1} = 0.1\mathrm{eV}, \mu_{c_2} = 0.16\mathrm{eV}$, T=3K, $\Gamma = 0.43\mathrm{meV}$, B=1T, D=8nm. (**a**,**b**) Faraday rotation angle in the far-field and transmission coefficient vs. frequency with a=b=6nm. (**c**,**d**) The same as previous one but with rectangular lattice with $a/b = 0.8$ and $ab = 36\mathrm{nm}^2$ - same fill factor as for the square lattice case. (**e**,**f**) The same as previous one but with $a/b = 1.25$ and $ab = 36\mathrm{nm}^2$ - same fill factor as for the square lattice case.